A new methodology for wheat attenuation correction at C-band VV-polarized backscatter time series

María Arias, Miguel Ángel Campo-Bescós, Luis Miguel Arregui, María González-Audícana and Jesús Álvarez-Mozos

***Abstract*— Wheat is one of the most important crops worldwide, and thus the use of remote sensing data for wheat monitoring has attracted much interest. Synthetic Aperture Radar (SAR) observations show that, at C-band and VV polarization, wheat canopy attenuates the surface scattering component from the underlying soil during a significant part of its growth cycle. This behavior needs to be accounted for or corrected before soil moisture retrieval is attempted. The objective of this paper is to develop a new method for wheat attenuation correction (WATCOR) applicable to Sentinel-1 VV time series and based solely on the information contained in the time series itself. The hypothesis of WATCOR is that without attenuation, VV backscatter would follow a stable long-term trend during the agricultural season, with short-term variations caused by soil moisture dynamics. The method relies on time series smoothing and changing point detection, and its implementation follows a series of simple steps. The performance of the method was compared by evaluating the correlation between backscatter and soil moisture content in six wheat fields with available soil moisture data. The Water Cloud Model (WCM) was also applied as a benchmark. The results showed that WATCOR successfully removed the attenuation in the time series, and achieved the highest correlation with soil moisture, improving markedly the correlation of the original backscatter. WATCOR can be easily implemented, as it does not require parameterization or any external data, only an approximate indication of the period where attenuation is likely to occur.**

***Index Terms*—wheat, attenuation, SAR, time series, soil moisture, Sentinel-1**

I. INTRODUCTION

Wheat is one of the most important crops at the global scale, being the main food grain source for humans [1]. The monitoring of major crops like wheat is essential for important applications such as food security assurance [2] or biomass and yield forecasting [3]. Soil moisture (SM) is one of the key variables subject to be monitored. The occurrence of plagues and diseases can be affected by SM, and it plays a key role in the development of crops as it determines the availability of water for plants [4]. At a global scale, SM is a key variable of the climate system and it is involved in a number of feedbacks affecting weather events [5].

In-situ probes can measure SM at the point scale, but generalizing point measurements to spatial areas is not straightforward due to its high spatial variability [6]. Therefore, remote sensing has received great interest, as a source of spatial information over large areas of the territory with a given periodicity. Microwave sensors are the most suitable for SM estimation, because at this wavelengths the soil response is determined partly by its dielectric properties that mainly depend on surface SM [7]. Operational global SM products at coarse resolution (25-50 km) have been developed in the last years, mainly based on radiometers [8]–[10] or scatterometers [11]. SAR sensors offer a finer spatial resolution (10-20 m), suitable for SM estimation at the agricultural field or irrigation sector scale. Nevertheless, these sensors are more severely affected by other variables such as soil surface roughness [12] or vegetation characteristics [13], and thus, SM retrieval at the field scale is still a challenging task [14], [15].

SAR based SM retrieval is a subject that has been studied for more than forty years [16]. Different models have been developed for bare soils over the years. The Integral Equation Model (IEM) [17] and the Advanced Integral Equation Model (AIEM) [18], [19] are physical-based models widely used [20], [21]. Semi-empirical models were also developed, such as Oh [22], Dubois [23] or Shi [20]. The inversion of these models allows estimating a variable (e.g. SM) from backscatter observations, knowing the rest of the variables of the model (e.g., surface roughness). Machine learning techniques have also been used for SM estimation, for instance artificial neural networks (ANN) [24] or support vector machines (SVM) [25], [26]. In some studies, machine learning approaches were trained using synthetic datasets generated with models, such as IEM [27], while in other cases training was performed with real remote sensing observations and in situ data [28].

The backscatter response from vegetation canopies is complex, as it is influenced by sensor configuration (e.g., frequency, wavelength and incidence angle), the physical structure and the dielectric properties of plant elements and the characteristics of the underlying soil. Therefore, SM estimation under vegetated surfaces requires the coupling of vegetation and soil backscatter models [29] in order to separate both

This work was supported by the Spanish Ministry of Science and Innovation through project PID2019-107386RB-I00 / AEI / 10.13039/501100011033 and doctoral grant (BES-2017-080560).

M. Arias, M.A. Campo-Bescós, M. González-Audicana and J. Álvarez-Mozos are with the Institute of Sustainability and Food Chain Innovation (IS-FOOD), Department of Engineering, Public University of Navarre (UPNA), Arrosadia Campus, 31006 Pamplona, Spain (e-mail: maria.arias@unavarra.es; jesus.alvarez@unavarra.es). L.M. Arregui is with the Institute of Sustainability and Food Chain Innovation (IS-FOOD), Department of Agricultural Engineering, Biotechnology and Food, Public University of Navarre (UPNA), Arrosadia Campus, 31006 Pamplona, Spain.

contributions. Different models that simulate the backscatter from canopies have been developed. Full electromagnetic scattering models, like the Michigan Microwave Canopy Scattering model (MIMICS) [30], [31], might be difficult to use in an operational setting due to the large number of parameters required. Therefore, approximate solutions like the semi-empirical Water Cloud Model (WCM) [32] have gained interest and popularity due to its relatively simplicity [7], [33]. The WCM represents the vegetation canopy as a medium composed of identical water particles that can be represented by bulk descriptors related to its density (e.g., Vegetation Water Content or LAI). For empirically fitting WCM coefficients, backscatter observations, SM measurements and vegetation descriptors are required. Different studies investigated alternative vegetation descriptors that might be obtained from in-situ data or from remote sensing observations [13], [27]. The first ones are costly and time consuming, while remote sensing based descriptors might be more easily obtained. The latter include optical vegetation indices (e.g., NDVI.) [34], [35] or features obtained from multi-pol SAR observations (crosspol ratio, etc.) [36], [37]. SAR features might be particularly interesting for areas where weather conditions preclude the use of optical data [36]. WCM simulates both the vegetation contribution to backscatter (volume scattering) and its effect in attenuating the soil contribution. It usually requires a specific parameterization for each vegetation type, vegetation descriptor and study site [38], which needs additional in situ-measurements for validation purposes.

Wheat canopy has a particular behavior in VV polarization, with a characteristic scattering dynamics during the different phenological stages [39], and a dominant scattering mechanism consisting of soil backscatter attenuated by the canopy [40]–[42]- At early stages backscatter mainly reflects the response of soil, since the crop development is still poor [43], [44]. Then, this soil backscatter component is attenuated gradually during the stem elongation phase due to the vertical structure of wheat plants, reaching its minimum values by the heading stage [40], when backscatter starts to increase. Then, during crop maturity and senescence, wheat plants dry out and the attenuation capacity of wheat canopy gradually diminishes leading to an increase in backscatter [45] until the crop is finally harvested. Ouaadi et al [46] proposed that the attenuation produced by wheat was the main cause of the scattered relationship between SM and backscatter, while Weiβ et al [47] found that the uncertainty in SM estimation increased from stem elongation until heading, coinciding with the period of attenuation.

An approach for attenuation correction that would not require external data or local-site parameterization would be of wide interest from the applications point of view. Detailed backscatter time series observed over wheat fields by ongoing missions with a systematic observation planning, like Sentinel-1, might be an invaluable information source for characterizing the attenuation behavior of wheat. This would allow designing and implementing data-driven approaches based on the backscatter time series itself. Therefore, the objectives of this paper are:

- To describe the backscattering behavior of wheat for C-band VV polarization using a large dataset of Sentinel-1 observations.
- To propose a new method for wheat attenuation correction (WATCOR) in VV polarization based solely on the backscatter time series itself.
- To evaluate the proposed approach and compare it with the state-of-the-art WCM using a dataset comprising in-situ SM measurements over several wheat fields.

The remaining of the article is structured in three separate sections, section II describes the general backscatter behavior of wheat, section III proposes the new method WATCOR and section IV evaluates and compares it with the WCM. Finally some conclusions are drawn.

II. General wheat behavior at C-band VV backscatter

This section analyzes a large wheat backscatter dataset collected during four agricultural campaigns (2016, 2017, 2018 and 2019) in Navarre (Spain). The objective is to describe the general backscatter behavior of this crop in VV polarization.

A. Methodology

1) Study area

The study area comprises the agricultural lands of the province of Navarre in Northern Spain (Figure 1). In spite of its relatively small extension (10,391 km^2), Navarre is characterized by its diversity regarding climate and landscape. The Northern area corresponds with the western side of the Pyrenees mountain range, and has a humid climate with a predominance of forests and prairies. In contrast, the Southern area, with a drier climate and a higher proportion of arable land, is formed by the plains of the Ebro basin. The transition zone between these two areas has mixed characteristics. This diversity leads to a stratification of Navarre in seven agricultural regions for administrative and management purposes. The detailed characteristics of the agricultural regions are described in Arias et al. [48]. Table I presents some basic features of the wheat fields therein.

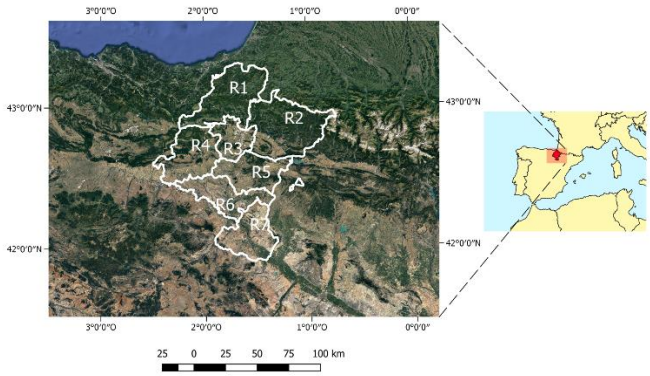

Fig. 1. Location of the province of Navarre and its seven agricultural regions

2) SAR imagery

Sentinel-1 C-band SAR imagery was the base for this study. Images were acquired in the Interferometric Wide (IW) swath mode with dual-pol (VH-VV) configuration, and they were downloaded as level-1 Ground Range Detected (GRD)

products. Sentinel-1 overpasses the study area in one ascending orbit (103ASC) and two descending orbits (8DESC and 81DESC). All available Sentinel-1A and B scenes in these three orbits covering the study area from 1 September 2015 to 31 August 2019 were used in this study, making a total of 563 scenes. The revisit time was variable during the years of study and the different orbits used. In 2016, S1B was not yet available so the revisit time was 12 days in all orbits, and then it shortened to 6 days for the rest of the study, except for orbit ASC103 where S1A was unavailable from April 2018 to the end of 2019.

The images were processed with an automated pipeline in SNAP Graph Processing Toolbox following these steps: 1) thermal noise removal; 2) slice assembly; 3) apply orbit file; 4) calibration; 5) speckle filtering (3x3 Gamma-Map); 6) terrain flattening; 7) range-doppler terrain correction and 8) subset to the extent of Navarre. After the process, γ^0 backscatter coefficients in dB units were obtained. The pixel size of the output products was set to 20 m. The SRTM 1sec HGT DEM was used for terrain flattening and terrain correction.

TABLE I
CHARACTERISTICS OF WHEAT FIELDS ON EACH AGRICULTURAL REGION

Agricultural region	Wheat area cultivated (ha)	Average size of fields (ha)	Average slope of fields (%)	Type of management
R1	583	1.03	12	Rainfed
R2	8126	1.83	11	Rainfed
R3	11620	1.73	11	Rainfed
R4	16990	1.39	11	Rainfed
R5	14941	1.47	9	Rainfed/Irrigated
R6	10348	1.55	5	Rainfed/Irrigated
R7	7695	1.73	6	Rainfed/Irrigated

3) Data extraction

The Agriculture Department of the Government of Navarre provided an anonymized version of the Land Parcel Information System (LPIS or SIGPAC in Spanish) with the crops declared for each parcel in the 2016, 2017, 2018 and 2019. This dataset consisted of a GIS polygon vector file and its corresponding attribute table with the crops stated by farmers in their EU Common Agricultural Policy (CAP) declarations. From this dataset, wheat parcels were extracted for each year and preprocessed as follows: (1) parcels smaller than 0.5 ha were discarded, (2) a 5 m inner buffer was applied to the parcel boundaries, (3) the median backscatter was computed for each parcel in each acquisition date leading to a backscatter time series for each parcel and year, and (4) the 10% of parcels most dissimilar to the characteristic wheat time series were discarded each year, since some CAP declarations might be erroneous [48]. The final number of wheat parcels used in this study was 21845 for 2016, 18750 for 2017, 20374 for 2018 and 20465 for 2019.

4) Analysis of the backscatter trend

For each agricultural region, year and satellite pass, the median VV backscatter time series of all wheat parcels were computed. Additionally, the median time series at the province level (Navarre) were also calculated. Each agricultural year started the 1st September of the previous year and ended the 31st August of the corresponding year.

Before analyzing the backscatter behavior of wheat, the similarity between years was evaluated by comparing the autocorrelation function (ACF) of the median time series. The ACF measures how fast or slowly data in the time series vary [49], and it is useful for identifying underlying trends in the time series. The correlation length (l_{cor}) was also calculated and used as a parameter that summarizes the information conveyed in the ACF. l_{cor} is the lag distance (days in our case) where autocorrelation in the time series is lost, this is commonly defined as the lag where the ACF falls below $1/e$ [50]. Finally, in order to evaluate the long-term backscatter trend, a moving average of 36 days was computed for the median time series. This process enables omitting rapid backscatter variations due to meteorological events or eventual agricultural practices, so that only the general backscatter trend caused by wheat canopy remains in the time series.

B. Autocorrelation results

Figure 2 showed that the ACFs obtained for the different years were similar, particularly during the first 50 lagged days. Autocorrelation values steadily decreased to a value of zero around day 100. Additionally, the ACF between the different orbit nodes was also quite similar, although orbit 103ASC had a slightly steeper decay.

When computing the ACFs for each agricultural region (Supplementary Materials 1), it can be observed that regions 6 and 7 presented a steeper decay than the rest, meaning that backscatter variations in wheat parcels of these regions might be more abrupt than in the other regions. The correlation length (Table II) enables comparing these ACFs quantitatively. Although there was some variability in l_{corr} between the different years studied, values did not deviate drastically from the mean (~30 days). The differences observed could be attributed as a first instance to the climatic conditions, with 2018 being the wettest year in the series for regions 4, 6 and 7 and showing lower l_{corr} values than the remaining years. In addition, Sentinel-1 revisit time was not consistent during the whole study period. 'It concurred that time series with lower temporal resolution (i.e., longer revisit time) had lower l_{corr}. Agricultural regions 6 and 7 showed lower l_{corr} values, probably due to the larger amount of irrigated wheat parcels in these regions that might result in a more dynamic SM variation (Supplementary Materials 1). The remaining regions had a very similar autocorrelation behavior to that observed at the provincial level. Altogether, this analysis demonstrates that wheat backscatter time series have a certain degree of autocorrelation that is similar every year, suggesting that wheat canopy creates an annual systematic trend in VV backscatter.

TABLE II
CORRELATION LENGTH OF MEDIAN WHEAT TIME SERIES ACF

Orbit node	Campaign 2016 (days)	Campaign 2017 (days)	Campaign 2018 (days)	Campaign 2019 (days)	Mean (days)
8DESC	25	28	34	37	31
81DESC	28	33	36	41	35
103ASC	22	29	27	27	26

C. *Long-term wheat backscatter trend analysis*

Figure 3 showed that backscatter slightly increased from September to November due to soil preparation and sowing. Also, November is normally a wet month, so the backscatter rise might respond to higher soil moisture. During December and January, backscatter values remain rather high (~-9.5dB). However, there was a clear decrease in backscatter from February to April, which reached its minimum value (~15dB) at the end of April. During this period, the vertical orientation of wheat canopy at the stem elongation stage (BBCH21-55) [51] produces an attenuation of backscatter [40]. Then, backscatter increased from April to June due to changes in the structure of plants, as a consequence of the successive phenological development, from flowering to ripening (BBCH55-99). Finally, after harvest, a stabilization in backscatter values was found in July and August (~12dB), when backscatter depends only on the bare soil response.

The smoothed time series of the different agricultural regions (Supplementary Materials 2) exhibited the same behavior with differences in their backscatter amplitude. For instance, the decrease in backscatter during attenuation reached ~6dB in northern regions, while in southern regions it was lower (~4dB). The duration of the attenuation period also varied, being longer in southern regions.

In summary, the analysis of the smoothed backscatter time series confirmed the existence of a seasonal trend caused by wheat canopy in VV backscatter, rather independent from SM variations and explained by wheat growth and phenology. Backscatter attenuation caused by the growth of vertical stems started approximately in February and lasted until the end of April, when the maximum attenuation was observed. Then, backscatter increased due to phenological development and later also due to the greater penetration when cereals are drying out during ripening and senescence, until harvest took place at the end of June. For individual fields, both the start and end of attenuation might be identified as changing points in their backscatter time series. The specific start and end points of attenuation for each parcel might vary due to the particular management and site conditions of the parcel.

III. A NEW METHOD FOR CORRECTING WHEAT ATTENUATION IN VV BACKSCATTER TIME SERIES

The previous section demonstrated that wheat canopy produces a particular backscatter pattern in VV polarization during the agricultural year. This section proposes a simple methodology for correcting wheat attenuation in VV backscatter time series (WATCOR), by using only information contained in the VV backscatter time series itself.

The initial hypothesis is that if no attenuation existed, VV backscatter would follow a rather stable long-term trend with backscatter variations mainly caused by surface roughness or moisture variations, as it occurs in the initial (Sep-Jan) and final (Jun-Aug) bare soil periods.

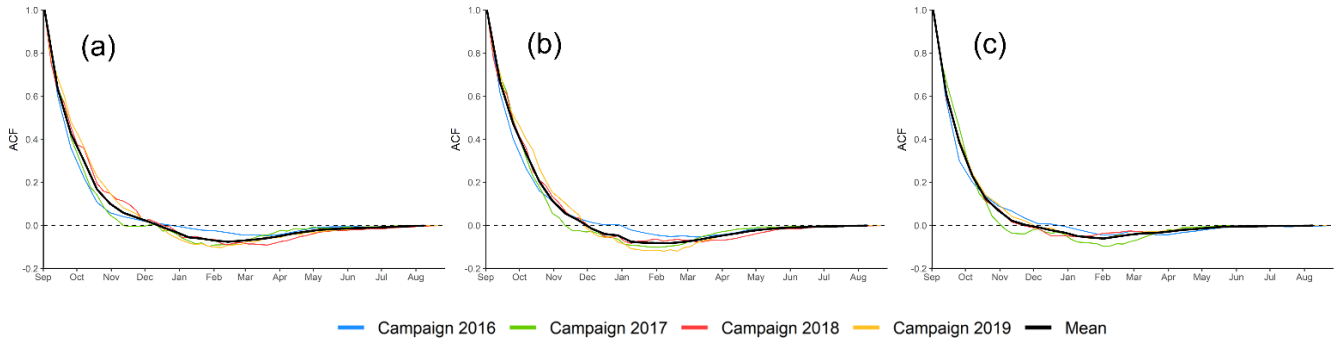

Fig. 2. Autocorrelation function (ACF) plots of median wheat time series in Navarre for the three different orbits: (a) 8DESC, (b) 81DESC and (c) 103ASC

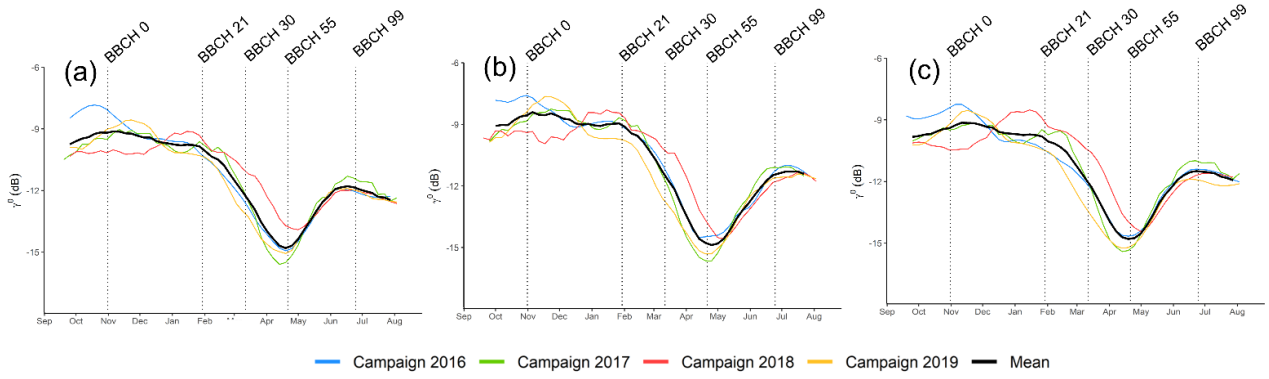

Fig. 3. Smoothed Sentinel-1 VV time series for the different agricultural campaigns and orbits: (a) 8DESC. (b) 81DESC. (c) 103ASC. Curves represent the median of all wheat parcels in Navarre. Main phenological stages (BBCH scale) are indicated.

The method follows a series of steps (Fig. 4). First, the period where attenuation occurs is identified. Then, a low frequency trend is interpolated for this period by assuming a linear transition from the start of the attenuation period to its end. Finally, the high frequency backscatter variations are finally added to the low frequency trend. These high frequency variations in the attenuation period are extracted by fitting and subtracting a lower envelope curve to the real backscatter time series. In the following subsections, these processes are explained in detail.

A. Low frequency backscatter trend extraction

The low frequency trend underlying VV backscatter time series was extracted by applying a Savitzky-Golay smoothing filter [45]. This filter considers that high frequency variations are noisy, and obtains a smoothed trend by computing a polynomial least-squares fit of order *p* inside a moving window of width *w* that crosses the signal [52]. The Savitzky-Golay filter requires a signal with constant frequency. Therefore, to comply with the missing scenes that seldom occur in Sentinel-1 time series, a daily linear interpolation was performed first. Then, the parameters of the filter were determined through visual interpretation. High values of *w* and low values of *p* produce smoother trends. The effects of varying these two parameters are displayed in Supplementary Materials 3. A polynomial order of one (p=1) with a window size of 45 days (w=45) yielded the best results, obtaining a smooth signal that preserved the attenuation trend and omitted high frequency backscatter dynamics.

B. Identification of the attenuation period

The period when wheat attenuated VV backscatter was identified by applying a change point detection technique in the smoothed backscatter series. Change points are points in the time series where unexpected and structural changes occur, changing the data properties such as the mean or the variance [53], [54]. Both the start and end of the attenuation period are changing points in the smoothed trend. Although the Savitzky-Golay smoothing minimized the number of changing points detected outside the attenuation period, some additional change points might be found, depending on other factors, such as the climatic conditions of the year. To avoid this, the change point search was constrained in time to periods where the start and end of attenuation are likely to happen. In our case, based on local knowledge, and the very high number of wheat parcels analyzed, the search was constrained to a 2-month period:

- Beginning of attenuation: from 15/Jan to 15/Mar.
- End of attenuation: from 15/May to 15/Jul.

These dates should be adjusted to the particular agricultural calendar and conditions of each site.

Once the search periods were set, a change point analysis algorithm [55] was applied, based on the statistical moments of the time series. The algorithm performed a nonparametric estimation of the number of change points and their position based on a divisive hierarchical clustering, without any additional assumption on their distribution. The algorithm parameters where set to k=1 (number of change points to estimate) and *min.size*=2 (minimum number of observations between change points).

C. Restitution of the smoothed trend

The smoothed backscatter trend was restituted to remove wheat attenuation. To achieve this, a linear trend was assumed between the start and end of the attenuation period (Fig.4b). Ideally, this restituted trend would follow the backscatter dynamics in case no attenuation existed.

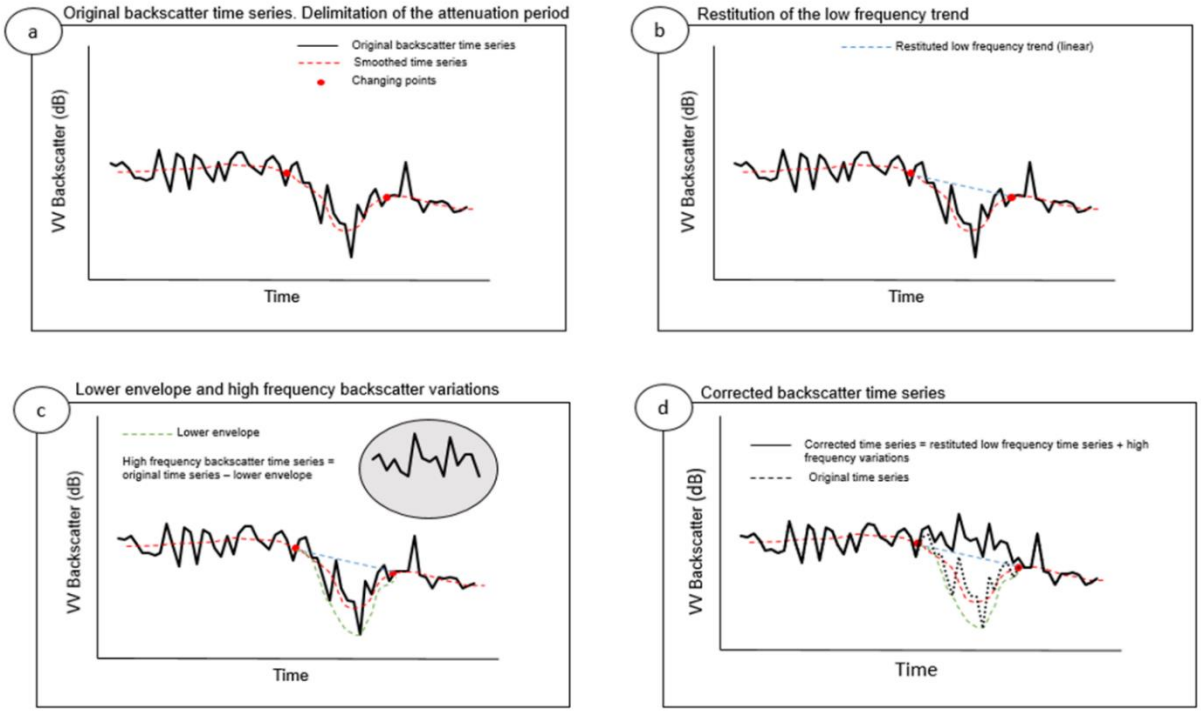

Fig. 4. Diagram indicating the main steps of WATCOR

D. Lower envelope determination

During the attenuation period, the lower envelope of the original backscatter time series represents the backscatter bottom line, with values above it that could correspond to soil wetting events. To extract this lower envelope, the iterative methodology of Chen et al. [56] was adapted to obtain a curve that fitted as good as possible the local minima in the backscatter time series. To automate the methodology six steps were followed (Fig.5):

1) Select the set of local minimum points in the backscatter time series (t, γ^0), through its first derivative. These points were flagged for later use as a reference $(t, \gamma^0)_{ref}$.
2) Smooth the time series using the Savitzky-Golay filter (parameters *p*=1, *w*=45), leading to a smoothed curve (t, γ^0_{s0}).
3) Initialization of an iteration ($k = 1, \dots, 100$). Remove high points in the time series, by selecting points that were above the smoothed curve and replacing their values with the ones on the smoothed curve (Eq.1). This way, a new backscatter time series was generated (t, γ^0_k),

$$\gamma^0_k = \begin{cases} \gamma^0, & \gamma^0 \leq \gamma^0_{sk-1} \\ \gamma^0_{sk-1}, & \gamma^0 > \gamma^0_{sk-1} \end{cases} \quad (1)$$

4) Smooth again the obtained backscatter time series (t, γ^0_k) using the Savitzky-Golay filter (parameters *p*=2, *w*=45), producing a newly smoothed backscatter time (t, γ^0_{sk}), which got closer to the lower envelope.
5) Compute a fitting index (F_k), as the RMSE between the reference points $(t, \gamma^0)_{ref}$ and their values in (t, γ^0_{sk}).
6) Steps 3-5 where iterated 100 times, and finally, the lower envelope was selected as the iteration (t, γ^0_{sk}) with the lowest F_k

E. Addition of high frequency backscatter variations to the restituted trend

The difference between the original backscatter time series and the lower envelope was calculated. This difference represented high frequency backscatter variations that mostly responded to soil wetting events. Therefore, it was added to the smoothed linear trend obtained in section C, resulting in the corrected backscatter time series, where wheat attenuation had been finally removed (Fig. 4d).

IV. Case Study: Backscatter and Soil Moisture Correlation

The aim of this last section is to evaluate the effectivity of the proposed approach (WATCOR) with a case study. Since the correction of the vegetation effect is a pre-requisite for many SM retrieval methods (e.g., IEM, Oh model, etc.), this evaluation was performed indirectly by measuring the correlation between SM measurements and VV backscatter time series before and after correction. With this aim, surface SM ground measurements obtained over wheat fields in three dedicated field campaigns were used. In addition, the proposed approach was compared with the well-known Water-Cloud Model (WCM) [32], implemented in three different variants. The rationale was that the method that best corrected vegetation influence should result in higher correlation values between backscatter and SM time series.

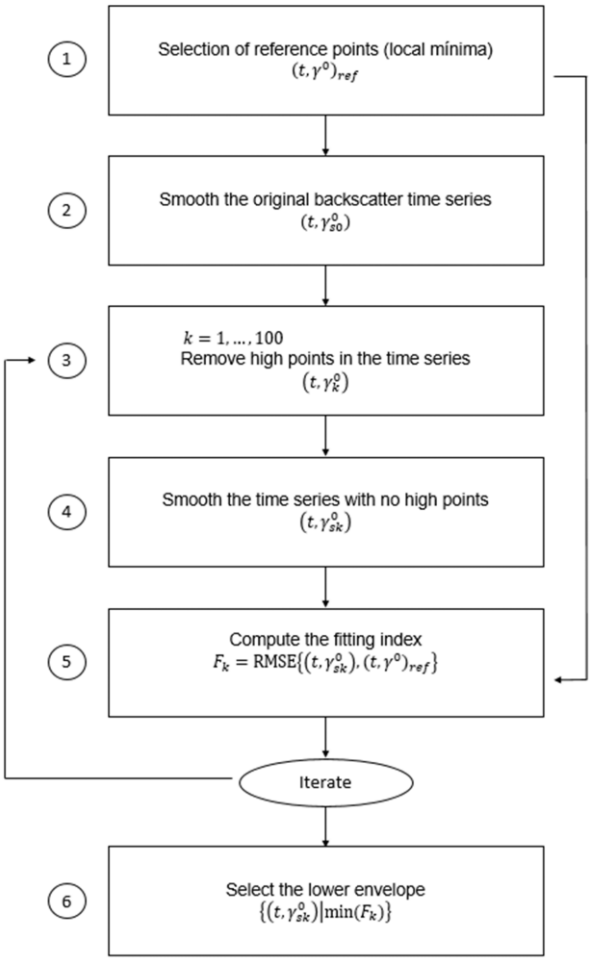

Fig. 5. Flowchart explaining the determination of the lower envelope

A. Methodology

1) Study area and soil moisture measurements

The study was conducted in six wheat fields located in the province of Navarre (Spain) (Fig. 6). The main characteristics of the fields are described in table III. From three to five capacitance SM probes (Sentek-multi) were installed on each field from winter until de end of June (harvest). The probes recorded the volumetric SM on a 30 minutes basis, at six different depths every 10cm, from the surface to 60cm deep, yet for this analysis only the surface layer (0-10cm) was considered. For each field, its SM time series was calculated as the median time series of the probes installed on it. Finally, from these field time series, a dataset was extracted with the SM measurements that coincided with Sentinel-1 acquisitions (Table IV).

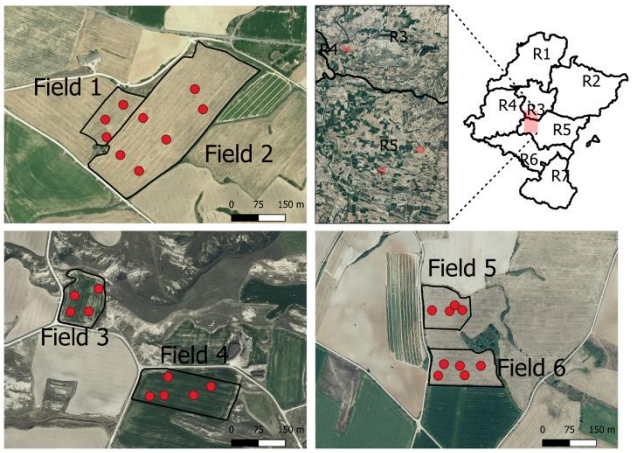

Fig. 6. Wheat fields location. Red dots represent the soil moisture probes

TABLE III
CHARACTERISTICS OF THE WHEAT FIELDS

Id	Area (ha)	Texture class	Type	Sowing date	Harvest	Number of probes
1	1.36	Clay-loam	Rainfed	25/10/2017	05/07/2018	3
2	8.50	Loam	Irrigated	25/10/2017	05/07/2018	6
3	1.57	Clay-loam	Rainfed	25/10/2018	06/07/2019	4
4	2.80	Silt-loam	Irrigated	25/10/2018	06/07/2019	5
5	1.37	Clay	Rainfed	11/12/2019	03/07/2020	4
6	1.86	Loam	Irrigated	11/12/2019	03/07/2020	5

TABLE IV
NUMBER OF SENTINEL-1 ACQUISITIONS PER ORBIT, AND START AND END DATES OF SM MEASUREMENTS

Id	8DESC	81DESC	103ASC	Initial date	Final date
1-2	20	21	13	03/03/2018	27/06/2018
3-4	19	20	9	14/02/2019	21/06/2019
5-6	29	29	29	31/12/2019	28/06/2020

2) Satellite imagery and data extraction

All available Sentinel-1 scenes from 1 September 2017 to 31 August 2020 were acquired and processed following the process explained in Section-II. After scene processing, a 10 m inner buffer was applied to the field boundaries and the median backscatter value for each field was computed on each of the Sentinel-1 acquisitions during its particular agricultural year (2018 for fields 1 and 2; 2019 for fields 3 and 4; and 2020 for fields 5 and 6). All backscatter data were normalized to a local incidence angle θ=40º, following the methodology explained in [57].

All available Sentinel-2 multispectral Level-2A Bottom of Atmosphere (BOA) reflectance images for the study period were also used, in this case obtained from Google Earth Engine. A subset of the study area was clipped, and scenes where the study fields were free of clouds were downloaded for further analysis. Two vegetation indices were computed: the normalized vegetation difference index (NDVI) [58] and the normalized water difference index (NDWI) [59]. As for Sentinel-1, median values were computed for each field, using the buffered polygon vector files, leading to field time series of NDVI and NDWI. Finally, a linear interpolation was applied to the NDVI and NDWI time series at a daily time step to derive a time series coincident with Sentinel-1 acquisitions.

3) WCM vegetation correction

The WCM is a semi-empirical model used to correct the vegetation influence on backscatter data [32]. The model describes vegetation as a 'cloud' composed of identical water droplets uniformly distributed within the canopy, which attenuates the microwave radiation, but might also contribute to the total backscatter [32]. The WCM is expressed as follows:

$$\sigma^0_{can} = \sigma^0_{veg} + \tau^2 \sigma^0_{soil} \quad (2)$$

$$\tau^2 = \exp(-\frac{2BV_2}{cos_\theta}) \quad (3)$$

$$\sigma^0_{veg} = AV_1 cos\theta (1 - \tau^2) \quad (4)$$

where σ^0_{can} is the total backscatter, σ^0_{veg} is the vegetation contribution; σ^0_{soil} is the soil contribution; τ^2 is a two-way attenuation factor; θ is the incidence angle; V_1 and V_2 are vegetation descriptors; and A and B are empirical parameters that depend on the vegetation descriptor and the radar configuration considered. It must be noted that in this study the WCM was fitted to VV polarized Sentinel-1 backscatter observations (in linear units) after terrain flattening, so γ^0 was used instead of σ^0.

In the literature, different vegetation descriptors for the WCM can be found, although V_1 and V_2 are usually considered the same (V_1=V_2). The most frequently used vegetation descriptors are: the vegetation water content (VWC) [60], the leaf area index (LAI) [61], the normalized vegetation difference index (NDVI) [13], the normalized water difference index (NDWI) [62] and to a lesser extent SAR descriptors, such as radar vegetation index (RVI) [36] or VH/VV ratio [37]. In this study, two optical-based WCM variants were implemented: one based on NDVI and the other on NDWI [59]. Additionally, a third WCM variant was used based on the VH/VV. VH/VV values, in linear units, were smoothed with Savitzky-Golay filter (p=1, w=45) and used as the SAR descriptor, from here onwards referred to as VH/VV, for simplicity.

Although some authors used given vegetation parameter values [63] in WCM, most studies determined the values of parameters A and B for each particular site through optimization [64] in a training scheme, where the soil component of backscatter (σ^0_{soil}) is an input. Some studies obtained σ^0_{soil} from physical backscattering models, such as the Integral Equation Model (IEM) [65] or Dubois model [66]. However, these models need additional field measurements, e.g. soil roughness. Alternatively, it can be assumed that σ^0_{soil} depends on volumetric soil moisture (SM) given [32]:

$$\sigma^0_{soil} = Dexp^{(SM \cdot C)} \quad (5)$$

where C and D are soil parameters depending on surface soil roughness and texture, respectively. In this study, only SM measurements were available and, therefore, equation 5 was used to obtain σ^0_{soil}. The only inputs used were: the VV backscatter time series in linear units (σ^0_{can}), the incidence angle, SM measurements and the vegetation descriptors considered on each variant. With this data, a non-linear

overdetermined system with four unknown parameters (A, B, C and D) was stablished [34]. The system was solved using the least-squared Powell's dog-leg algorithm [67], establishing the conditions that A and B are positive.

To train and validate the WCM a six-fold cross-validation scheme was implemented, which allowed to obtain A, B, C and D parameters for all fields, and state-of-the-art model performance metrics: RMSE, Pearson correlation (R) and BIAS [68]. Model train and validation was done separately for each WCM variant (NDVI, NDWI and VH/VV), assuming similar soil texture and roughness for all fields. For each case, the final validation results were the mean performance metrics of the six folds. The parameters of the models and the validation results can be found in Supplementary Materials 4.

Once the WCM parameters were obtained, σ^0_{soil} was extracted from equation (2) for each case, which represented the soil backscatter contribution corrected for the vegetation effect.

4) Correlation analysis

A correlation analysis was carried out to evaluate the performance of the vegetation correction methodologies investigated. For this, the original VV backscatter time series and the time series corrected with the proposed approach and the three WCM variants were correlated with the ground measured SM values, using Pearson correlation coefficient R.

Additionally, the correlation between short-term backscatter changes with sort-term SM changes was explored, since some SM retrieval methods are based on change detection techniques [69]. For this, the Pearson correlation coefficient of the backscatter difference between subsequent Sentinel-1 observations ($\Delta\gamma^0$) and their SM difference (ΔSM) was evaluated.

B. Results and discussion

1) Dynamics of the vegetation descriptors

The dynamics of NDVI and NDWI were quite similar (Fig. 7), increasing right after sowing. They reached a saturation plateau that extended until vegetation ripening [70]. This plateau was shorter for fields 5 and 6 because they were sown later, and thus had a shorter cycle. On the other hand, the dynamics of VH/VV time series were slightly different. VH/VV started to increase later, illustrating sensitivity to vegetative growth until mid-April approximately [71]–[73]. Then, there was a variable behavior at the end of the cycle. NDVI can be considered a proxy of biomass [13] and NDWI a proxy of VWC [74]. VH/VV ratio was also found to be a good proxy of crop biomass [72].

2) Corrected backscatter time series

Figure 8 shows the time series of all fields for 8DESC orbit (the results for the other two orbits are in Supplementary Materials 5). Although the amount of rainfall in spring was high, backscatter in the original time series decreased, demonstrating once again the attenuation caused by wheat in this period. The corrected time series presented differences according to the methodology applied. Focusing on WCM corrections, the first variant (NDVI) lead to significantly higher backscatter values since sowing. Similarly, the third variant (VH/VV) also resulted in higher values right after sowing. In both cases, the differences with the original time series increased with wheat development. Before harvest, the differences decreased for NDVI, but for VH/VV they remained relatively high in most fields. In the second variant (NDWI) the differences between the original backscatter time series and the corrected ones were lower. In this case, backscatter remained almost the same during the initial and last stages of the cycle, and variations only affected the attenuation period. After WCM correction with any of the three variants, it was still possible to possible to distinguish a residual attenuation in most fields (Fig. 8).

The differences between the three WCM variants were based in the differences between the vegetation descriptors. In general, the optical corrected backscatter series started to increase too early in the season, even before the attenuation period started. Then, due to the loss of sensitivity to further vegetation growth in the plateau, the moment of maximum attenuation was not adequately corrected. Finally, in the ripening stage, vegetation indices decreased rapidly leading to a sudden drop of backscatter. This behavior was more marked in the WCM variant with NDVI than with NDWI, since the latter produced a smaller correction. The WCM based on VH/VV produced a similar result and was not able to completely correct wheat attenuation at the maximum attenuation point.

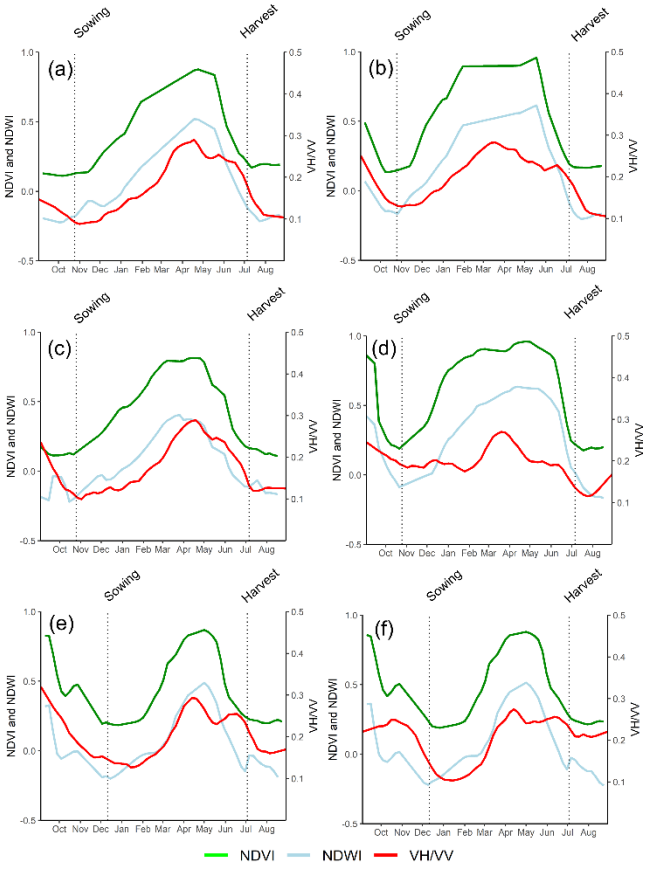

Fig. 7. Vegetation indices time series used as vegetation descriptors in WCM. (a) Field 1, (b) Field 2, (c) Field 3, (d) Field 4, (5) Field 5and (f) Field 6. For VH/VV data from orbit 8DESC is represented, the other two have a very similar pattern.

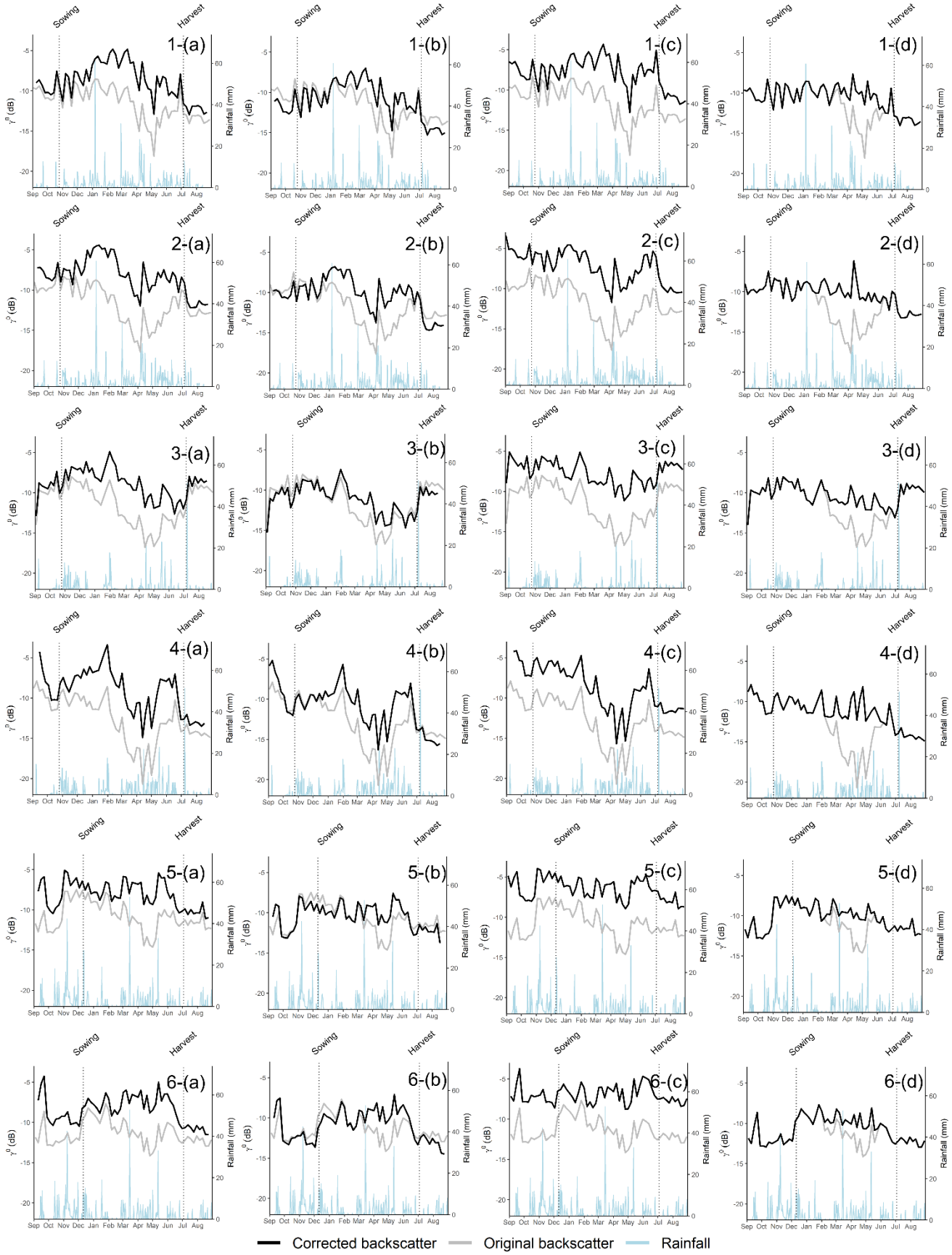

Fig. 8. Original and corrected backscatter time series for fields 1-6 for orbit 8DESC. The backscatter corrections are: (a) WCM-NDVI, (b) WCM-NDWI, (c) WCM-VH/VV and (d) WATCOR. Rainfall includes irrigation in irrigated fields

WATCOR, compared to the WCM variants investigated, only corrected backscatter values during the attenuation period, and the correction effect was smoother than that achieved with the WCM, in particular during the beginning of the season, when sudden variations in vegetation descriptors (in particular NDVI) lead to rapid changes. Furthermore, the new method adequately corrected the backscatter values at the highest attenuation point, compared to WCM corrections that were unable to completely correct it and resulted in a residual attenuation in this period.

3) Correlation results

The correlation coefficients obtained between backscatter and ground measured SM are displayed in figure 9. Additionally, scatterplots in figure 10 show the correlation obtained for all the fields together. Both figure 9 and 10 represent the correlation between γ^0 and SM and that of $\Delta\gamma^0$ and ΔSM. Further correlation results are given in Supplementary Materials 6

Regarding the correlation between γ^0 and SM, the original backscatter time series had the lowest results (Fig. 9a), with a median R value of 0.14. In this case, individual R values obtained for the different fields and orbit passes varied strongly; with several fields even leading to negative correlations, while only a couple of fields achieved R values above 0.5. The WCM corrections based on optical data (NDVI and NDWI) improved the original correlation values, with a median value ~0.30, being the NDVI correction slightly superior to the NDWI one. The individual results (Supplementary Materials 6) showed evidence that in most cases NDVI and NDWI had similar correlations. Other studies found that variants based on NDWI achieved better SM estimations than the ones on NDVI [35], [63], attributing this result to the higher sensitivity of the SWIR channel to the vegetation water content, and the low sensitivity of NDVI to further vegetation growth after an NDVI of 0.8 [65]. Conversely, Zhang et al. [29] obtained limited results with NDWI in dense wheat parcels with a modified version of the WCM, attributing this result to an eventual saturation to further increases in vegetation water content.

The correction based on the VH/VV ratio yielded lower R values, with a median value of 0.24, being only superior to the optical corrections in a few fields. The use of VH/VV as a vegetation descriptor in the WCM is appealing, as it could provide a means for correction with no need of external (optical) data. However, not many studies attempted this, and results were rather poor, with better results being achieved with NDVI at L-Band over wheat [75] and wetlands [37].

WATCOR achieved the highest correlations, with a median value R=0.47 (Fig. 9a). The method succeeded at increasing the correlation in most fields-orbits, with a couple of exceptions where it gave similar results to the original time series. Comparing WATCOR with the second best correction (NDVI), its performance was better in most cases. One of the exceptions was field 1, where correlation values were already high regardless of the correction applied, so differences between WCM and WATCOR were small. It must be admitted, that in some fields, in particular the two fields monitored in 2019, correlation results were low in all cases, suggesting that some external factors (e.g., soil stoniness or a later sowing) might be playing a role.

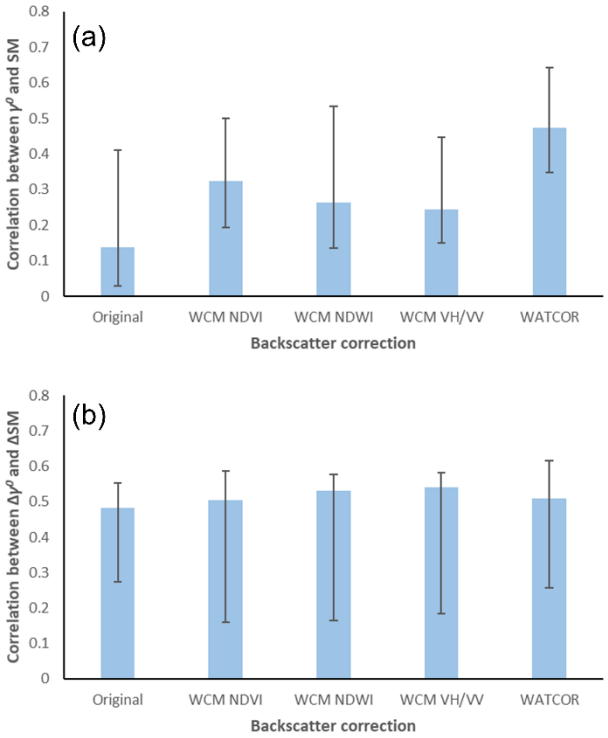

Fig. 9. Median correlation results, (a) correlation between backscatter and SM, (b) correlation between backscatter differences ($\Delta\gamma^0$) and SM differences (ΔSM) between consecutive days. Error bars represent the first and third quartile.

When comparing the results obtained with the different orbits (Supplementary Materials 6), it can be seen that 103ASC produced poorer result in 2019, which might be due to the longer revisit time (due to the unavailability of Sentinel-1A in this orbit for that particular year), and hence a reduced sample for model fitting and correlation evaluation. In contrast, WATCOR achieved higher correlation values for 103ASC in 2018 (revisit time 6 to 12 days); and 2020 (6 days). Image acquisition in descending orbits was at early morning hours where dew was often present, which could affect backscatter [76] and its correlation with SM. WATCOR specially succeed at improving the correlation for irrigated fields compared with rain-fed ones, although it is not easy to grasp why.

Exploring the scatterplots of Figure 10(a-e), it can be observed that the original time series (a) had many low backscatter values (<-15dB) regardless of the SM value of that moment. All the vegetation corrections applied were successful at reducing this effect. Overall, the γ^0-SM correlation values always increased when a vegetation correction was applied, which confirms the necessity for correcting backscatter observations before attempting to retrieve SM over wheat fields.

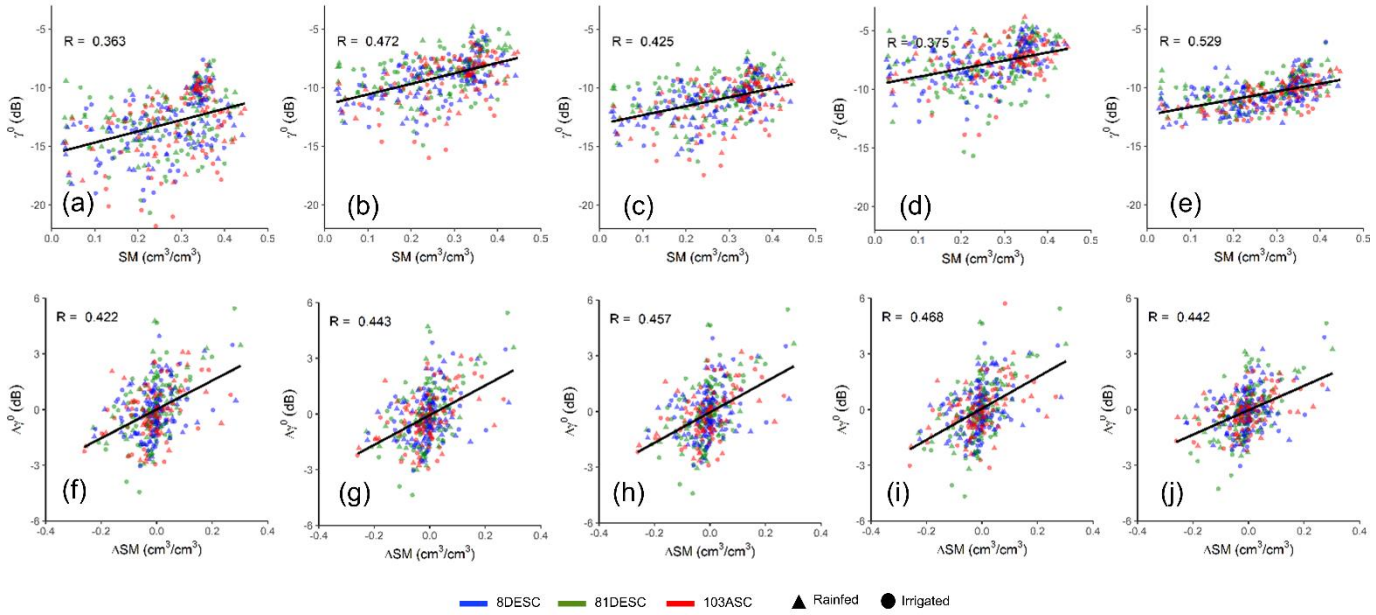

Fig. 10. Dependence of backscatter on volumetric soil moisture for all sub-fields: absolute values (upper row) and differences between consecutive values (lower row); for the different backscatter correction investigated (a, f) original backscatter, (b, g) WCM-NDVI, (c, h) WCM-NDWI, (d, i) WCM-VH/VV (d, j) WATCOR

Concerning the $\Delta\gamma^0$ and ΔSM correlation, it appeared that all the explored casuistry achieved similar general results. The scatterplots in figure 10(f-j) showed a similar behavior and correlation values in figure 9b (~0.51) showed no improvements after vegetation correction. Therefore, these results suggest that vegetation correction might not be necessary when applying SM retrieval methods based on change detection techniques (e.g., [63]), at least if the temporal resolution is ~6 days

These results indicate that WATCOR can be useful for correcting wheat attenuation at C-band VV backscatter time series (e.g., Sentinel-1), before SM is retrieved with methods designed for bare soil conditions [77], [78]. The method proposed is based on sound time series analysis techniques like time series smoothing and changing point identification. Time series smoothing has been previously applied for a plethora of remote sensing applications that rely on multitemporal observations, such as crop phenology monitoring [79], [80], reconstruction of missing data [56], land-cover classification [81] or for obtaining high quality vegetation descriptors for climate modelling [82]. The results obtained might change if the parameters of the S-G filter were different. In this study, these parameters were selected through visual interpretation. Yet, in future studies, it would be interesting to devise an objective criterion for their selection, e.g. through cal/val schemes using additional ground truth SM datasets.

WATCOR assumes that the effect of wheat in VV backscatter is a smooth, low frequency trend, and its application requires little user intervention. It is simple, does not require external data and the results obtained even overpassed the WCM. Furthermore, unlike the WCM, WATCOR does not require any model parameterization. The only input required is the specification of approximate beginning and end dates of the attenuation period, and therefore, a previous knowledge of the study area regarding the phenological development of wheat. Therefore, the approach can be easily implemented in automatized pipelines, as a preprocessing step before SM estimation is attempted However, WATCOR relies on the whole backscatter time series, and in its present form cannot be applied in real-time. Further research is needed to improve this.

The underlying idea of WATCOR, i.e., to extract a low-frequency trend that is later subtracted from the original backscatter time series, could be transferred to other types of crops. However, this would require specific adaptations depending on the particular backscatter behavior of each crop. Furthermore, additional research is recommended to test the applicability of WATCOR at other microwave bands, as the signal penetration into the vegetation canopy is different.

V. Conclusion

In this paper, the backscatter behavior of wheat for C-band VV polarization was analyzed as a pre-requisite for the development of a methodology for correcting the attenuation from vegetation. A large dataset containing EU CAP declarations from farmers of four agricultural campaigns in a region (Navarre) with a high diversity of agro-climatic conditions was used. The performance of the new correction was evaluated with an analysis of the correlation between backscatter and volumetric soil moisture. The correlation was compared to WCM corrections based on optical and radar vegetation descriptors.

The results revealed that wheat time series had a typical seasonal trend, independent from soil moisture variations, with wheat plants mainly attenuating VV polarized backscatter from phenological stage BBCH21 until harvest. The behavior was identical for different agro-climatic regions, with only some differences in the amplitude of attenuation. Using standard techniques of time series smoothing and changing point detection, it was possible to identify the start and end of the attenuation period, where the proposed method, WATCOR, was applied.

The corrected time series showed that WATCOR could effectively remove the attenuation pattern, while the time series obtained with WCM still presented a certain degree of attenuation. After correcting the vegetation effect, correlations between backscatter and soil moisture improved in all cases, with WATCOR obtaining the best general performance. Looking at results in detail, it appeared that the temporal resolution of the time series affected the results, with poorer results being observed for ASC103 pass in 2019, where revisit time was 12 days.

Overall, WATCOR provided good results and might be an alternative to other vegetation correction methods for wheat. The method does not account for the direct backscatter contribution of vegetation, contrary to the WCM, but the results suggest that this effect might be neglected in wheat, at least at C-band and VV polarization. The main advantage of the method proposed is that it does not require external information or any model parametrization. It only needs an approximate prior knowledge on the period where attenuation is likely to occur in a specific region or site. However, it relies on the whole time series of radar backscatter, making it difficult to correct the attenuation in real-time In the near future, the application of this method for soil moisture estimation techniques should be evaluated.

ACKNOWLEDGMENT

The authors would like to acknowledge the Government of Navarre for providing the (CAP) declarations database used in this research.

REFERENCES

[1] "Food and Agriculture Organization of the United Nations. FAOSTAT," https://www.fao.org/faostat/en/#data/QCL, 2021. .

[2] K. Van Tricht, A. Gobin, S. Gilliams, and I. Piccard, "Synergistic use of radar Sentinel-1 and optical Sentinel-2 imagery for crop mapping: a case study for Belgium," Remote Sens., pp. 1–22, 2018.

[3] S. C. Steele-Dunne, H. McNairn, A. Monsivais-Huertero, J. Judge, P. W. Liu, and K. Papathanassiou, "Radar remote rensing of agricultural canopies: A review," *IEEE J. Sel. Top. Appl. Earth Obs. Remote Sens.*, vol. 10, no. 5, pp. 2249–2273, 2017.

[4] H. Vereecken, J. A. Huisman, H. Bogena, J. Vanderborght, J. A. Vrugt, and J. W. Hopmans, "On the value of soil moisture measurements in vadose zone hydrology: A review," *Water Resour. Res.*, vol. 46, no. 4, pp. 1–21, 2010.

[5] S. I. Seneviratne *et al.*, "Investigating soil moisture-climate interactions in a changing climate: A review," *Earth-Science Rev.*, vol. 99, no. 3–4, pp. 125–161, 2010.

[6] T. E. Ochsner *et al.*, "State of the art in large-scale soil moisture monitoring," *Soil Sci. Soc. Am. J.*, vol. 77, no. 6, pp. 1888–1919, 2013.

[7] K. C. Kornelsen and P. Coulibaly, "Advances in soil moisture retrieval from synthetic aperture radar and hydrological applications," *J. Hydrol.*, vol. 476, pp. 460–489, 2013.

[8] Y. H. Kerr *et al.*, "The SMOS soil moisture retrieval algorithm," *IEEE Trans. Geosci. Remote Sens.*, vol. 50, no. 5 PART 1, pp. 1384–1403, 2012.

[9] S. K. Chan *et al.*, "Assessment of the SMAP Passive Soil Moisture Product," *IEEE Trans. Geosci. Remote Sens.*, vol. 54, no. 8, pp. 4994–5007, 2016.

[10] L. Brocca *et al.*, "Soil moisture estimation through ASCAT and AMSR-E sensors: An intercomparison and validation study across Europe," *Remote Sens. Environ.*, vol. 115, no. 12, pp. 3390–3408, 2011.

[11] V. Naeimi, K. Scipal, Z. Bartalis, S. Hasenauer, and W. Wagner, "An improved soil moisture retrieval algorithm for ERS and METOP scatterometer observations," *IEEE Trans. Geosci. Remote Sens.*, vol. 47, no. 7, pp. 1999–2013, 2009.

[12] N. E. C. Verhoest, H. Lievens, W. Wagner, J. Álvarez-Mozos, M. S. Moran, and F. Mattia, "On the soil roughness parameterization problem in soil moisture retrieval of bare surfaces from synthetic aperture radar," *Sensors*, vol. 8, no. 7, pp. 4213–4248, 2008.

[13] R. Bindlish and A. P. Barros, "Parameterization of vegetation backscatter in radar-based, soil moisture estimation," *Remote Sens. Environ.*, vol. 76, no. 1, pp. 130–137, 2001.

[14] W. Wagner *et al.*, "Operational readiness of microwave remote sensing of soil moisture for hydrologic applications," *Hidrol. Res.*, vol. 38, no. 1, pp. 1–20, 2007.

[15] J. Peng *et al.*, "A roadmap for high-resolution satellite soil moisture applications – confronting product characteristics with user requirements," *Remote Sens. Environ.*, vol. 252, p. 112162, 2021.

[16] H. C. Macdonald and W. P. Waite, "Soil Moisture Detection with Imaging Radars," *Water Resour. Res.*, vol. 7, no. 1, pp. 100–110, 1971.

[17] A. K. Fung, *Microwave Scattering and Emission Models and their Applications*. Artech House Publishers, 1994.

[18] A. K. Fung and K. S. Chen, "An update on the IEM surface backscattering model," *IEEE Geosci. Remote Sens. Lett.*, vol. 1, no. 2, pp. 75–77, 2004.

[19] K. L. Chen, K. S. Chen, Z. L. Li, and Y. Liu, "Extension and validation of an advanced integral equation model for bistatic scattering from rough surfaces," *Prog. Electromagn. Res.*, vol. 152, no. July, pp. 59–76, 2015.

[20] J. Shi, J. Wang, A. Y. Hsu, P. E. O'Neill, and E. T. Engman, "Estimation of bare surface soil moisture and surface roughness parameter using L-band SAR image data," *IEEE Trans. Geosci. Remote Sens.*, vol. 35, no. 5, pp. 1254–1266, 1997.

[21] J. Kong, J. Yang, P. Zhen, J. Li, and L. Yang, "A coupling model for soil moisture retrieval in sparse vegetation covered areas based on microwave and optical remote sensing data," *IEEE Trans. Geosci. Remote Sens.*, vol. 56, no. 12, pp. 7162–7173, 2018.

[22] Y. Oh, K. Sarabandi, and F. T. Ulaby, "An Empirical Model and an Inversion Technique for Radar Scattering from Bare Soil Surfaces," *IEEE Trans. Geosci. Remote Sens.*, vol. 30, no. 2, pp. 370–381, 1992.

[23] P. Dubois, J. van Zyl, and T. Engman, "Measuring Soil Moisture with Imaging Radars," *IEEE Trans. Geosci. Remote Sens.*, vol. 33, no. 6, pp. 915–926, 1995.

[24] A. Hachani, M. Ouessar, S. Paloscia, E. Santi, and S. Pettinato, "Soil moisture retrieval from Sentinel-1 acquisitions in an arid environment in Tunisia: application of Artificial Neural Networks techniques," *Int. J. Remote Sens.*, vol. 40, no. 24, pp. 9159–9180, 2019.

[25] S. Ahmad, A. Kalra, and H. Stephen, "Estimating soil moisture using remote sensing data: A machine learning approach," *Adv. Water Resour.*, vol. 33, no. 1, pp. 69–80, 2010.

[26] L. Pasolli *et al.*, "Estimation of soil moisture in mountain areas using SVR technique applied to multiscale active radar images at C-band," *IEEE J. Sel. Top. Appl. Earth Obs. Remote Sens.*, vol. 8, no. 1, pp. 262–283, 2015.

[27] M. El Hajj, N. Baghdadi, M. Zribi, and H. Bazzi, "Synergic use of Sentinel-1 and Sentinel-2 images for operational soil moisture mapping at high spatial resolution over agricultural areas," *Remote Sens.*, vol. 9, no. 12, pp. 1–28, 2017.

[28] F. Greifeneder, C. Notarnicola, and W. Wagner, "A machine learning-based approach for surface soil moisture estimations with google earth engine," *Remote Sens.*, vol. 13, no. 11, 2021.

[29] M. Zhang, F. Lang, and N. Zheng, "Soil moisture retrieval during the wheat growth cycle using sar and optical satellite data," *Water (Switzerland)*, vol. 13, no. 2, pp. 1–19, 2021.

[30] F. T. Ulaby, K. Sarabandi, K. McDonald, M. Whitt, and M. C. Dobson, "Michigan microwave canopy scattering model," *Int. J. Remote Sens.*, vol. 11, no. 7, pp. 1223–1253, 1990.

[31] R. J. Brown, B. G. Brisco, and G. Edwards, "Adaptation of the MIMICS

Backscattering Model to the Agricultural Context—Wheat and Canola at L and C Bands," *IEEE Trans. Geosci. Remote Sens.*, vol. 32, no. 1, pp. 47–61, 1994.

[32] E. P. W. Attema and F. T. Ulaby, "Vegetation modeled as a water cloud," *Radio Sci.*, vol. 13, no. 2, pp. 357–364, 1978.

[33] A. J. Graham and R. Harris, "Extracting biophysical parameters from remotely sensed radar data: A review of the water cloud model," *Prog. Phys. Geogr.*, vol. 27, no. 2, pp. 217–229, 2003.

[34] W. Zhuo *et al.*, "Assimilating Soil Moisture Retrieved from Sentinel-1 and Sentinel-2 Data into WOFOST Model to Improve Winter Wheat Yield Estimation," *Remote Sens.*, vol. 11, no. 13, p. 1618, 2019.

[35] Y. Bao, L. Lin, S. Wu, K. A. Kwal Deng, and G. P. Petropoulos, "Surface soil moisture retrievals over partially vegetated areas from the synergy of Sentinel-1 and Landsat 8 data using a modified water-cloud model," *Int. J. Appl. Earth Obs. Geoinf.*, vol. 72, no. June, pp. 76–85, 2018.

[36] J. Li and S. Wang, "Using SAR-derived vegetation descriptors in a water cloud model to improve soil moisture retrieval," *Remote Sens.*, vol. 10, no. 9, pp. 11–14, 2018.

[37] K. Dabrowska-Zielinska *et al.*, "Soil moisture in the Biebrza Wetlands retrieved from Sentinel-1 imagery," *Remote Sens.*, vol. 10, no. 12, 2018.

[38] J. Álvarez-Mozos, J. Casalí, M. González-Audícana, and N. E. C. Verhoest, "Assessment of the operational applicability of RADARSAT-1 data for surface soil moisture estimation," *IEEE Trans. Geosci. Remote Sens.*, vol. 44, no. 4, pp. 913–923, 2006.

[39] J. M. Stiles, K. Sarabandi, and F. T. Ulaby, "Electromagnetic scattering from grassland-part II: measurement and modeling results," *IEEE Trans. Geosci. Remote Sens.*, vol. 38, no. 1 II, pp. 349–356, 2000.

[40] F. Mattia *et al.*, "Multitemporal C-band radar measurements on wheat fields," *IEEE Trans. Geosci. Remote Sens.*, vol. 41, no. 7 PART I, pp. 1551–1560, 2003.

[41] S. C. M. Brown, S. Quegan, K. Morrison, J. C. Bennett, and G. Cookmartin, "High-resolution measurements of scattering in wheat canopies - Implications for crop parameter retrieval," *IEEE Trans. Geosci. Remote Sens.*, vol. 41, no. 7 PART I, pp. 1602–1610, 2003.

[42] H. Skriver, M. Thoug, and A. G, "Multitemporal C- and L-Band Polarimetric Signatures of Crops," *IEEE Trans. Geosci. Remote Sens.*, vol. 37, no. 5, pp. 2413–2429, 1999.

[43] A. Larranaga, J. Alvarez-Mozos, L. Albizua, and J. Peters, "Backscattering behavior of rain-fed crops along the growing season," *IEEE Geosci. Remote Sens. Lett.*, vol. 10, no. 2, pp. 386–390, 2013.

[44] K. Harfenmeister, D. Spengler, and C. Weltzien, "Analyzing temporal and spatial characteristics of crop parameters using Sentinel-1 backscatter data," *Remote Sens.*, vol. 11, no. 13, pp. 1–30, 2019.

[45] C. Liu, J. Shang, P. W. Vachon, and H. McNairn, "Multiyear crop monitoring using polarimetric RADARSAT-2 data," *IEEE Trans. Geosci. Remote Sens.*, vol. 51, no. 4, pp. 2227–2240, 2013.

[46] N. Ouaadi *et al.*, "C-band radar data and in situ measurements for the monitoring of wheat crops in a semi-Arid area (center of Morocco)," *Earth Syst. Sci. Data*, vol. 13, no. 7, pp. 3707–3731, 2021.

[47] T. Weiß, T. Ramsauer, T. Jagdhuber, A. Löw, and P. Marzahn, "Sentinel-1 backscatter analysis and radiative transfer modeling of dense winter wheat time series," *Remote Sens.*, vol. 13, no. 12, pp. 1–25, 2021.

[48] M. Arias, M. A. Campo-Bescós, and J. Alvarez-Mozos, "Crop Classification Based on Temporal Signatures of Sentinel-1 Observations over Navarre Province, Spain," *Remote Sens.*, pp. 1–29, 2020.

[49] P. M. T. Broersen, *Automatic Autocorrelation and Spectral Analysis*. Springer, 2006.

[50] F. T. Ulaby, R. K. Moore, and A. K. Fung, *Microwave Remote Sensing: Active and Passive*, Vol II. Boston, MA: Reading, MA: Addison-Wesley, 1982.

[51] P. D. Lanchashire *et al.*, "A uniform decimal code for growth stages of crops and weeds," *Ann. Appl. Biol.*, vol. 119, no. 3, pp. 561–601, 1991.

[52] A. Savitzky and M. J. E. Golay, "Smoothing and Differentiation of Data by Simplified Least Squares Procedures," *Anal. Chem.*, vol. 36, no. 8, pp. 1627–1639, 1964.

[53] S. Sharma, D. A. Swayne, and C. Obimbo, "Trend analysis and change point techniques: a survey," *Energy, Ecol. Environ.*, vol. 1, no. 3, pp. 123–130, 2016.

[54] A. F. Militino, M. Moradi, and M. D. Ugarte, "On the performances of trend and change-point detection methods for remote sensing data," *Remote Sens.*, vol. 12, no. 6, pp. 1–25, 2020.

[55] D. S. Matteson and N. A. James, "A nonparametric approach for multiple change point analysis of multivariate data," *J. Am. Stat. Assoc.*, vol. 109, no. 505, pp. 334–345, 2014.

[56] J. Chen, P. Jönsson, M. Tamura, Z. Gu, B. Matsushita, and L. Eklundh, "A simple method for reconstructing a high-quality NDVI time-series data set based on the Savitzky-Golay filter," *Remote Sens. Environ.*, vol. 91, no. 3–4, pp. 332–344, 2004.

[57] I. E. Mladenova, T. J. Jackson, R. Bindlish, and S. Hensley, "Incidence angle normalization of radar backscatter data," *IEEE Trans. Geosci. Remote Sens.*, vol. 51, no. 3, pp. 1791–1804, 2013.

[58] J. W. Rouse, R. H. Haas, J. A. Schell, and D. W. Deering, "Monitoring vegetation systems in the Great Plains with ERTS," in *S.C. Freden, E.P. Mercanti, and M. Becker (eds) Third Earth Resources Technology Satellite-1 Syposium. Volume I: Technical Presentations, NASA SP-351, NASA, Washington, D.C.*, 1974, no. 1, pp. 309–317.

[59] B.-C. Gao, "NDWI - A normalized Difference Water Index for Remote Sensing of Vegetation Liquid Water From Space," *Remote Sens. Environ.*, vol. 58, no. 3, pp. 257–266, 1996.

[60] E. Ayari, Z. Kassouk, Z. Lili-Chabaane, N. Baghdadi, S. Bousbih, and M. Zribi, "Cereal crops soil parameters retrieval using L-band ALOS-2 and C-band sentinel-1 sensors," *Remote Sens.*, vol. 13, no. 7, 2021.

[61] M. El Hajj *et al.*, "Soil moisture retrieval over irrigated grassland using X-band SAR data," *Remote Sens. Environ.*, vol. 176, pp. 202–218, 2016.

[62] X. Chai, T. Zhang, Y. Shao, H. Gong, L. Liu, and K. Xie, "Modeling and mapping soil moisture of plateau pasture using RADARSAT-2 imagery," *Remote Sens.*, vol. 7, no. 2, pp. 1279–1299, 2015.

[63] Q. Wang *et al.*, "Comparative Analysis of Landsat-8, Sentinel-2, and GF-1 Data for Retrieving Soil Moisture over Wheat Farmlands," *Remote Sens.*, vol. 12, no. 2708, pp. 1–16, 2020.

[64] J. Álvarez-Mozos, J. Casalí, M. González-Audícana, and N. E. C. Verhoest, "Correlation between ground measured soil moisture and RADARSAT-1 derived backscattering coefficient over an agricultural catchment of Navarre (North of Spain)," *Biosyst. Eng.*, vol. 92, no. 1, pp. 119–133, 2005.

[65] N. Baghdadi, M. El Hajj, M. Zribi, and S. Bousbih, "Calibration of the Water Cloud Model at C-Band for winter crop fields and grasslands," *Remote Sens.*, vol. 9, no. 9, pp. 1–13, 2017.

[66] M. Xing *et al.*, "Retrieving surface soil moisture over wheat and soybean fields during growing season using modified water cloud model from RADARSAT-2 SAR data," *Remote Sens.*, vol. 11, no. 16, 2019.

[67] M. J. . Powell, "A new algorithm for unconstrained optimization," *Nonlinear Program.*, pp. 31–66, 1970.

[68] Y. Han, X. Bai, W. Shao, and J. Wang, "Retrieval of soil moisture by integrating Sentinel-1A and MODIS data over agricultural fields," *Water (Switzerland)*, vol. 12, no. 6, 2020.

[69] A. Balenzano, F. Mattia, G. Satalino, and M. W. J. Davidson, "Use of dense temporal series of C-band SAR data for soil moisture retrieval over agricultural sites," *IEEE J. Sel. Top. Appl. Earth Obs. Remote Sens.*, vol. 4, no. 2, pp. 439–450, 2011.

[70] H. Lawrence *et al.*, "Comparison between SMOS Vegetation Optical Depth products and MODIS vegetation indices over crop zones of the USA," *Remote Sens. Environ.*, vol. 140, pp. 396–406, 2014.

[71] M. Meroni *et al.*, "Comparing land surface phenology of major European crops as derived from SAR and multispectral data of Sentinel-1 and -2," *Remote Sens. Environ.*, vol. 253, no. December 2020, 2021.

[72] A. Veloso *et al.*, "Understanding the temporal behavior of crops using Sentinel-1 and Sentinel-2-like data for agricultural applications," *Remote Sens. Environ.*, vol. 199, pp. 415–426, 2017.

[73] S. Khabbazan *et al.*, "Crop Monitoring Using Sentinel-1 Data: A Case Study from The Netherlands," *Remote Sens.*, vol. 11, no. 16, p. 1887,

2019.

[74] T. J. Jackson *et al.*, "Vegetation water content mapping using Landsat data derived normalized difference water index for corn and soybeans," *Remote Sens. Environ.*, vol. 92, no. 4, pp. 475–482, 2004.

[75] Z. Wang, T. Zhao, J. Qiu, X. Zhao, R. Li, and S. Wang, "Microwave-based vegetation descriptors in the parameterization of water cloud model at L-band for soil moisture retrieval over croplands," *GIScience Remote Sens.*, vol. 58, no. 1, pp. 48–67, 2021.

[76] D. Wood, H. McNairn, R. J. Brown, and R. Dixon, "The effect of dew on the use of RADARSAT-1 for crop monitoring: Choosing between ascending and descending orbits," *Remote Sens. Environ.*, vol. 81, no. 2–3, p. 456, 2002.

[77] A. K. Fung, Z. Lee, and K. S. Chen, "Backscattering from a Randomly Rough Dielectric Surface," *IEEE Trans. Geosci. Remote Sens.*, vol. 30, no. 2, pp. 356–369, 1992.

[78] B. Bauer-Marschallinger *et al.*, "Toward Global Soil Moisture Monitoring with Sentinel-1: Harnessing Assets and Overcoming Obstacles," *IEEE Trans. Geosci. Remote Sens.*, vol. 57, no. 1, pp. 520–539, 2019.

[79] F. Canisius *et al.*, "Tracking crop phenological development using multi-temporal polarimetric Radarsat-2 data," *Remote Sens. Environ.*, vol. 210, no. September 2017, pp. 508–518, 2018.

[80] M. Schlund and S. Erasmi, "Sentinel-1 time series data for monitoring the phenology of winter wheat," *Remote Sens. Environ.*, vol. 246, no. December 2019, p. 111814, 2020.

[81] Y. Shao, R. S. Lunetta, B. Wheeler, J. S. Iiames, and J. B. Campbell, "An evaluation of time-series smoothing algorithms for land-cover classifications using MODIS-NDVI multi-temporal data," *Remote Sens. Environ.*, vol. 174, pp. 258–265, 2016.

[82] H. Yuan, Y. Dai, Z. Xiao, D. Ji, and W. Shangguan, "Reprocessing the MODIS Leaf Area Index products for land surface and climate modelling," *Remote Sens. Environ.*, vol. 115, no. 5, pp. 1171–1187, 2011.

María Arias received the B.Sc degree in Agricultural Engineering and the M.Sc degree in GIS and Remote Sensing from the Public University of Navarre (UPNA), Spain, in 2014 and 2017, respectively. She is currently working toward her Ph.D degree at the Department of Engineering of the Public University of Navarre. Her research is focused on the estimation of variables of interest for agriculture from SAR remote sensing at the field scale.

Miguel Ángel Campo-Bescós received the degree in Agricultural Engineering and the PhD in Rural and Environmental Engineering, from the Public University of Navarre (UPNA), Spain, in 2003 and 2011, respectively. During his doctoral thesis, he was visiting student at the Department of Civil and Environmental Engineering ofthe Massachusetts Institute of Technology. He was a postdoctoral researcher at the Department of Agricultural and Biological Engineering University of Florida. Currently, he is Assistant Professor in the Department of Engineering at UPNA. He is also researcher at the Institute for Sustainability & Food Chain Innovation (IS-FOOD). His lines of research focus on the study and modeling of soil erosion and irrigation science, with special interest in the adoption and integration of new technologies. He has participated in 16 research projects, funded by international, national and regional public calls. In addition, he has participated in 15 technology transfer projects, being the principal investigator in 10 of the 15. He has over 150 contributions in indexed international journals, book chapters and conference contributions, in the field of Agricultural and environmental Sciences.

Luis Miguel Arregui received the degree in Agricultural Engineering and the PhD in Agronomy, from the Public University of Navarre (UPNA), Spain, in 1994 and 2006, respectively. Currently, he is Assistant Professor at the Department of Agronomy, Biotechnology and Food at UPNA and researcher at the Institute for Sustainability & Food Chain Innovation (IS-FOOD), UPNA. His research interests are varied and cover the physiology, agronomy and management aspects of crop production, as well as the application of technological innovations, such as soil moisture sensors and remote sensing, for a smart agriculture, both in irrigated and rainfed areas. He has participated as researcher or main researcher in 23 projects with public or private funds. His research works have been published in nearly 40 journal papers, book chapters and conferences contributions.

María González-Audícana received the M.S. and Ph.D. degrees in agricultural engineering from the Public University of Navarre, Pamplona, Spain, in 1996 and 2001, respectively. She was an Assistant Professor from 1997 to 2007. Since 2007, she has been an Associate Professor with the Department of Projects and Rural Engineering, Public University of Navarre. She is currently involved in research activities on remote sensing data preprocessing, multisensor data fusion and image spectral and textural classification for agricultural management purposes.

Jesús Álvarez-Mozos received the Engineering and Ph.D. degrees in agricultural engineering from the Public University of Navarre (UPNA), Pamplona, Spain, in 2001 and 2006, respectively. He was a Teaching Assistant from 2001 to 2010 with the Department of Projects and Rural Engineering, UPNA, where he later became an Associate Professor in 2011 with the Department of Engineering. His main research interest include remote sensing and its applications to agriculture and hydrology, although he has also worked on issues related to soil water erosion and hydrological modelling. An important part of his work focused on SAR remote sensing and more especially on the estimation of soil moisture and other variables of agricultural interest, such as soil roughness, crop type or crop condition. He has participated in more than 15 research projects funded by national or regional institutions, being the Principal Investigator in 4 of them. He has successfully supervised 4 PhD students, and published more than 40 research articles. His appointment at UPNA also consists of teaching tasks, since 2015 he is the Academic Director of a Master in GIS and Remote Sensing.